HHS Public Access

Author manuscript

Nat Neurosci. Author manuscript; available in PMC 2009 October 01.

Published in final edited form as:

Nat Neurosci. 2009 April ; 12(4): 454–462. doi:10.1038/nn.2289.

Phosphodiesterase 1C is dispensable for rapid response termination of olfactory sensory neurons

Katherine D. Cygnar and **Haiqing Zhao**

Department of Biology, The Johns Hopkins University, 3400 North Charles Street, Baltimore, MD 21218

Abstract

In the nose, odorants are detected on the cilia of olfactory sensory neurons (OSNs), where a cAMP-mediated signaling pathway transforms odor stimulation into electrical responses. Phosphodiesterase (PDE) activity in OSN cilia was long thought to account for rapid response termination by degrading odor-induced cAMP. Two PDEs with distinct cellular localization have been found in OSNs: PDE1C in cilia; PDE4A throughout the cell but absent from cilia. We disrupted both genes in mice and performed electroolfactogram analysis. Unexpectedly, eliminating PDE1C did not prolong response termination. Prolonged termination occurred only in mice lacking both PDEs, suggesting that cAMP degradation by PDE1C in cilia is not a rate-limiting factor for response termination in wildtype. *Pde1c*$^{-/-}$ OSNs instead displayed reduced sensitivity and attenuated adaptation to repeated stimulation, suggesting potential roles for PDE1C in regulating sensitivity and adaptation. These observations provide new perspectives in regulation of olfactory transduction.

INTRODUCTION

In vertebrates, olfactory sensory neurons (OSNs) use a cyclic AMP (cAMP) second messenger-mediated signal transduction pathway to convert odor stimulation into electrical signals. Olfactory signal transduction takes place on the cilia extending from the dendritic knob of the OSN1, 2. Odor exposure leads to elevated activity of Adenylyl Cyclase III (ACIII), resulting in a rapid rise of the cAMP concentration in the cilia. cAMP directly opens olfactory cyclic nucleotide-gated (CNG) ion channels, resulting in influx of Ca^{2+} and Na^{+} and membrane depolarization3, 4. Ca^{2+} can then open Ca^{2+}-activated Cl^{-} channels, which results in efflux of Cl^{-} and further depolarization, contributing to the generation of action potentials5–8.

In cyclic nucleotide-mediated signal cascades, the magnitude and duration of second messenger signals are determined by the activities of two opposing enzymes: the cyclase for the production and the phosphodiesterase (PDE) for the degradation of cyclic nucleotides. In olfactory transduction, PDE activity in the cilia has long been thought to account for rapid

Correspondence should be addressed to H.Z. (hzhao@jhu.edu).

termination of the OSN response by degrading odor-induced cAMP9, 10, leading to the closure of CNG channels. Two distinct cyclic nucleotide PDEs, PDE1C11, 12 and PDE4A13, 14, have been identified in mammalian OSNs. PDE1C is a Ca^{2+}/calmodulin-stimulated PDE11; PDE4A is Ca^{2+} insensitive but has substrate specificity for cAMP15. Immunohistochemical staining revealed that the PDE1C protein is selectively enriched in the cilia, while the PDE4A protein is distributed throughout the cell, including the dendritic knob from where the cilia emanate, but is absent from the cilia13, 14, 16. PDE1C was therefore hypothesized to be critical for rapid termination of the OSN response due to its cilial localization and Ca^{2+} dependency, while PDE4A was not expected to affect OSN responses as it is excluded from the cilia.

To assess the function of PDE1C and PDE4A in olfactory transduction, we disrupted both the *Pde1c* and the *Pde4a* gene in mice and conducted electrophysiological analysis of OSN responses using electroolfactogram (EOG). Loss of PDE1C was predicted to prolong response termination. Contrary to the expectation, eliminating PDE1C alone resulted in accelerated termination of the EOG response. Prolonged response termination occurred only in mice lacking both PDE1C and PDE4A, revealing that the activity of either PDE1C in the cilia or PDE4A outside of the cilia is sufficient to allow rapid termination of the EOG response. These results suggest that in wildtype OSNs cAMP degradation by PDE1C in cilia is not a rate-limiting factor for response termination. We found that *Pde1c*$^{-/-}$ OSNs instead display reduced sensitivity to odors and attenuated adaptation to repeated stimulation.

RESULTS

Generation of *Pde1c*$^{-/-}$ and *Pde4a*$^{-/-}$ mice

We took a loss-of-function approach to examine the role of phosphodiesterases in olfactory transduction. We generated mouse lines in which the *Pde1c* and *Pde4a* genes are disrupted individually and in combination (Supplementary Fig. 1 online). This genetic approach allows specific and complete elimination of the targeted PDE activity, a condition not achievable with current pharmacological inhibitors. Both individual knockout mice and *Pde1c*$^{-/-}$;*Pde4a*$^{-/-}$ double knockout mice show apparently normal growth rate and feeding, nursing, and mating behaviors.

We confirmed the loss of PDE1C and PDE4A proteins in the relevant knockout strains by immunohistochemistry (Fig. 1a). In wildtype olfactory epithelium (OE), PDE1C is detected primarily in the cilial layer, whereas PDE4A is detected in OSN cell bodies, dendrites, and axons. PDE1C and/or PDE4A immunoreactivity is absent in the relevant mutant mice. The thickness of the OE at similar nasal positions is comparable between all genotypes, and all genotypes show similar immunostaining for other olfactory transduction components, including ACIII and the CNG channel subunit CNGB1b, and for GAP43 (immature OSN marker) and OMP (mature OSN marker) (Fig. 1a). The loss of either PDE does not affect the localization of the other PDE, i.e. in *Pde1c*$^{-/-}$ mice, the localization of PDE4A protein is normal, and vice versa (Fig. 1a and Fig 3a). However, we found that there is a significant reduction in the level of ACIII protein in *Pde1c*$^{-/-}$ and *Pde1c*$^{-/-}$;*Pde4a*$^{-/-}$ olfactory epithelium as examined by Western blotting (Fig. 1b). The level of CNGB1b protein in these mice appears unchanged.

Pde1c$^{-/-}$ OSNs show smaller responses and faster termination

To determine the function of PDE1C in olfactory transduction, we recorded EOG signals from *Pde1c*$^{-/-}$ and wildtype mice in response to 100 ms odor pulses. The EOG has been widely used as a reliable and convenient means to assess OSN responses17, 18 and is thought to result primarily from the summed generator potentials of OSNs, although it may also have other components. We used two common odorants, amyl acetate and heptaldehyde, and analyzed four metrics of the EOG signal: the amplitude, the response latency, the rise time, and the rate of response termination. Similar results were obtained for both odorants. We present the data for amyl acetate in the main text, and provide quantification of the responses to heptaldehyde in Supplementary Table 1 online.

Eliminating PDE1C, the only PDE known in the cilia, was expected to prolong response termination. It may also allow for larger responses with quicker onset as cAMP concentrations could increase more rapidly when degradation of cAMP is reduced. Contrary to expectations, *Pde1c*$^{-/-}$ mice displayed faster response termination compared to the wildtype (Fig. 2b). The rate of response termination was quantified by calculating the time constant (τ) through fitting the decay phase of the EOG signal with a single exponential equation. The termination τ of *Pde1c*$^{-/-}$ mice were smaller than those of the wildtype for all odorant concentrations tested (Fig. 2c and Table 1, which lists data for 10^{-4}, 10^{-3} and 10^{-2} M amyl acetate). *Pde1c*$^{+/-}$ heterozygous mice displayed responses no different from the wildtype (Supplementary Fig. 2 online).

Pde1c$^{-/-}$ mice also displayed significantly reduced EOG amplitudes with slower onset kinetics. The maximum EOG amplitude of *Pde1c*$^{-/-}$ mice (9.8 ± 2.5 mV, n = 5 mice) was approximately half of that of the wildtype (21.4 ± 3.9 mV, n = 7 mice) (Fig. 2a). Both the response latency, defined as the time between the initiation of the odor pulse and the start of the response (1% of EOG peak value), and the rise time, defined as the time from the start of the response to the peak, are significantly longer in *Pde1c*$^{-/-}$ mice (Fig. 2d,e and Table 1). The reduced response magnitude, slower onset kinetics, and faster response termination observed in *Pde1c*$^{-/-}$ mice are reminiscent of OSNs in a state of cellular adaptation.

PDE1C knockout eliminates all PDE activity from OSN cilia

Since *Pde1c*$^{-/-}$ mice did not show the expected prolonged response termination, it raised a question whether there is additional PDE activity in the *Pde1c*$^{-/-}$ cilia responsible for removal of cAMP. Our initial characterization of *Pde1c*$^{-/-}$ mice showed that PDE4A, the only other PDE found in OSNs, remained localized in the dendrite and cell body but not in the cilial layer (Fig. 1a). We further confirmed this observation with double-label immunofluorescence comparing anti-PDE4A staining with that for the cilia marker acetylated tubulin. PDE4A and acetylated tubulin antibodies labeled distinct spatial domains in the OE of both wildtype and *Pde1c*$^{-/-}$ mice (Fig. 3a).

We also carried out a PDE catalytic activity assay on preparations of OSN cilia (Fig. 3b). PDE activity in OSN cilia is known to be stimulated by Ca^{2+} and calmodulin (CaM)16, which has been attributed to the Ca^{2+}/CaM sensitivity of PDE1C11. We measured PDE activity in wildtype and *Pde1c*$^{-/-}$ cilia preparations under three conditions: in a standard

reaction buffer containing no Ca^{2+} (0 mM Ca^{2+} and 0.1 mM EGTA); in the reaction buffer supplemented with 200 μM Ca^{2+} and 50 nM CaM; and in the reaction buffer supplemented with a broad-range PDE inhibitor 3-isobutyl-1-methylxanthin (IBMX, 0.5 mM). Wildtype preparations exhibited PDE activity in the absence of Ca^{2+} (1.5 ± 0.33 nmol mg^{-1} min^{-1}), reflecting the basal PDE activity in the cilia. When the buffer is supplemented with Ca^{2+} and CaM, wildtype cilial PDE activity is increased ~2.3-fold (3.4 ± 0.60 nmol mg^{-1} min^{-1}), consistent with a previous report16. IBMX blocked all cilial PDE activity (0.17 ± 0.50 nmol mg^{-1} min^{-1}). In *Pde1c*$^{-/-}$ cilia preparations, no basal PDE activity was detected in the standard reaction buffer (0.08 ± 0.21 nmol mg^{-1} min^{-1}), nor did the addition of Ca^{2+}/CaM elicit any PDE activity (0.002 ± 0.16 nmol mg^{-1} min^{-1}). In both conditions the activity levels were similar to those when IBMX was added (0.02 ± 0.23 nmol mg^{-1} min^{-1} for *Pde1c*$^{-/-}$ cilia). We conclude that knocking out PDE1C eliminated all PDE activity from OSN cilia.

Pde4a$^{-/-}$ OSNs display no aberrant response properties

To address whether PDE4A influences OSN responses, we measured EOG signals in *Pde4a*$^{-/-}$ mice using the same odorants and stimulation protocols as for *Pde1c*$^{-/-}$ mice. No differences were observed between *Pde4a*$^{-/-}$, *Pde4a*$^{+/-}$ and wildtype mice in any aspect of the EOG signal (Fig. 4 and Supplementary Fig. 2). These results are consistent with the idea that because PDE4A is excluded from the cilia, its impact on olfactory transduction may be minimal under most circumstances.

Pde1c$^{-/-}$;*Pde4a*$^{-/-}$ OSNs show prolonged response termination

Previous electrophysiological experiments showed that treatment of OSNs with IBMX prolonged OSN responses to odors, indicating degradation of cAMP by PDE activity is essential for rapid response termination9. However, neither *Pde1c*$^{-/-}$ nor *Pde4a*$^{-/-}$ mice displayed prolonged termination of EOG signals, suggesting that in these mutant mice the rate of cilial cAMP removal is still adequate to allow rapid response termination. As IBMX is a broad-range PDE inhibitor, treatment would inhibit simultaneously both PDE1C and PDE4A, a situation which would reflect a *Pde1c*$^{-/-}$;*Pde4a*$^{-/-}$ double knockout.

We generated *Pde1c*$^{-/-}$;*Pde4a*$^{-/-}$ mice and performed EOG recordings. These mice displayed a significantly prolonged response termination for all odorant concentrations tested (Fig. 5a,b and Table 1). This result suggests that removal of cAMP from the cilia is substantially impaired when both PDEs are not functional, consistent with previous studies using IBMX to eliminate all PDE activity9. In addition, *Pde1c*$^{-/-}$;*Pde4a*$^{-/-}$ mice displayed significantly reduced EOG amplitudes and slower onset kinetics compared to the wildtype (Fig. 5c). The reduction in EOG amplitudes and the extended latency of responses in the double knockout mice are comparable to those of *Pde1c*$^{-/-}$ mice. The increase in the response rise time in double knockout mice is even greater than that in *Pde1c*$^{-/-}$ mice (Supplementary Fig. 3 online).

Given the additive effect of the double knockout on response kinetics, we further examined *Pde1c*$^{-/-}$;*Pde4a*$^{+/-}$, *Pde1c*$^{+/-}$;*Pde4a*$^{-/-}$, *and Pde1c*+/−;*Pde4a*$^{+/-}$ mice. We did not observe any significant genetic dosage effects, as *Pde1c*$^{-/-}$;*Pde4a*+/− mice show responses

similar to *Pde1c*$^{-/-}$ mice, and both *Pde1c*$^{+/-}$;*Pde4a*$^{-/-}$ and *Pde1c*$^{+/-}$;*Pde4a*$^{+/-}$ mice show responses similar to the wildtype (Supplementary Fig. 2 and Supplementary Table 2 online).

Pde1c$^{-/-}$;*Pde4a*$^{-/-}$ mice also displayed significantly larger baseline noise of the EOG signal than the wildtype (Fig. 5d,e). The baseline noise was quantified as the standard deviation in the voltage during 2 s of baseline recording (2 kHz sampling rate). The increase in baseline noise likely reflects an increase in sporadic opening of CNG channels due to spontaneously generated cAMP, which cannot be quickly removed from the cilia of double knockout mice. *Pde1c*$^{-/-}$ mice displayed only a trend of increased baseline noise; the difference from wildtype is not significant.

OSN adaptation is differently affected in the mutant mice

Adaptation, the phenomena of decreasing responses either to repeated stimuli or during sustained stimuli, is a characteristic feature of OSN responses. Both forms of adaptation are thought to rely on different but overlapping sets of mechanisms19, 20. Due to its Ca^{2+}/CaM sensitivity, PDE1C has long been hypothesized to contribute to OSN adaptation11, 12, 20. Ca^{2+}, which enters cilia as part of the OSN response, can bind CaM and subsequently elevate PDE1C activity. If the stimulation continues or a subsequent stimulation occurs while PDE1C activity is elevated, the amount of cAMP available to open the CNG channel would be reduced, leading to smaller responses (i.e. adaptation). However, it has been previously reported that OSNs display a similar extent of adaptation to repeated stimulation when stimulated with intracellular delivery of either cAMP or non-hydrolyzable cAMP analogs, suggesting that the combined activity of all PDEs does not play a role in adaptation to repeated stimulation21. The function of individual PDEs in OSN adaptation has not been directly examined.

To assess the role of PDE1C and PDE4A in OSN adaptation to repeated odor exposure, we recorded EOG signals from mice bearing single or combined mutations of *Pde1c* and *Pde4a* using a paired-pulse protocol, which consisted of two identical 100 ms odor pulses separated by a 1 s interpulse interval (Fig. 6a). The extent of adaptation is quantified as the ratio of the 2nd "net" peak amplitude (see Methods for details) to the 1st peak amplitude18. *Pde1c*$^{-/-}$ mice still displayed adaptation, but with significant attenuation. The ratios of 2nd to 1st pulse response were significantly larger compared to the wildtype for all concentrations tested (Fig. 6b). These data suggest PDE1C likely contributes to OSN adaptation to repeated stimulation.

Paired-pulse protocols with interpulse intervals of 2, 4, 6, and 8 s were also examined (Supplementary Fig. 3 online). As the interpulse interval lengthened, the response amplitude to the 2nd pulse progressively recovered. When the interpulse interval was 4 s or longer, there were no differences in the ratios of 2nd to 1st pulse responses between *Pde1c*$^{-/-}$ and wildtype mice, indicating the influence of PDE1C on adaptation is limited to a short period following stimulation.

Pde4a$^{-/-}$ mice displayed adaptation indistinguishable from wildtype (Fig. 6a,b). Interestingly, *Pde1c*$^{-/-}$;*Pde4a*$^{-/-}$ mice also did not show a deficit in adaptation, despite the fact that *Pde1c*$^{-/-}$ mice have attenuated adaptation. This observation in double knockouts is

consistent with the previous report that OSNs did not display apparent deficits in adaptation to repeated stimulation when all PDE activity is bypassed21.

To assess the role of PDE1C and PDE4A in OSN adaptation during sustained odor exposure, we recorded EOG signals in response to a 10 s odor pulse (Fig. 6c). During the pulse, the EOG amplitude progressively declined in all genotypes. The extent of adaptation was quantified as the percentage of amplitude decline relative to the peak amplitude at the 10 s time point. Neither *Pde4a*$^{-/-}$ nor, interestingly, *Pde1c*$^{-/-}$ displayed deficits in adaptation during sustained stimulation, although the longer response latency and rise time are still evident in *Pde1c*$^{-/-}$ mice (Fig. 6c,d). In contrast, however, *Pde1c*$^{-/-}$*;Pde4a*$^{-/-}$ double knockout mice display significantly less decline during the course of stimulation (Fig. 6c,d). For 10^{-3} M amyl acetate (Fig. 6c), the response of *Pde1c*$^{-/-}$*;Pde4a*$^{-/-}$ mice declined approximately 27%, whereas wildtype and single knockout mice declined approximately 55%. This decreased response decline is consistent with the idea that cilial cAMP removal is substantially impaired when both PDE1C and PDE4A are eliminated.

DISCUSSION

Rapid response termination after a stimulus is critical to allow sensory neurons to represent the temporal information of the stimulus, and to be prepared for subsequent stimulation. In OSNs, rapid response termination has long been thought to rely substantially on degradation of cAMP in the cilia. However, *Pde1c*$^{-/-}$ OSNs, despite the lack of all cilial PDE activity, do not display prolonged termination. This result suggests that other mechanism(s) must be able to efficiently remove cAMP from cilia in the absence of cilial degradation. The most reasonable mechanism is that cAMP diffuses from the cilia into the dendritic knob and dendrite, where it can be degraded by PDE4A. These two mechanisms for cilial cAMP removal—degradation in the cilia and diffusion away from the cilia followed by degradation in the dendrite—are illustrated in Supplementary Fig. 5. Indeed, cAMP diffusion in olfactory cilia has been measured to be nearly as fast as diffusion in water (2.7×10^{-6} cm^2 s^{-1}, ref. 22). Computer modeling using this value together with published values of PDE enzyme activities shows that diffusion of cAMP from the cilia followed by degradation in the knob can occur within the time scale of termination of EOG responses (Fig. 7, and Supplementary note online). cAMP degradation (or sequestration) in the dendritic knob is required for efficient flux of cAMP away from the cilia, since the dendritic knob is not large enough to be an effective sink for cAMP (given the knob volume is approximately equal to the total volume of all the cilia of an OSN). In the absence of both cilial and dendritic degradation (as in *Pde1c*$^{-/-}$*;Pde4a*$^{-/-}$ OSNs), removal of cilial cAMP is severely hindered, leading to prolonged response termination.

In OSNs, rapid response termination depends on the closing of both CNG channels and Ca^{2+}-activated Cl^- channels. Removal of odor-evoked cAMP, in addition to feedback inhibition by Ca^{2+}/CaM18, 23, leads to closing of CNG channels, while removal of cilial Ca^{2+} leads to closing of the Cl^- channels24. The slowest of these processes would be the rate-limiting factor for response termination. When cAMP can be degraded in the cilia (as in wildtype or *Pde4a*$^{-/-}$ OSNs), cAMP removal will be faster than when cAMP can only be removed by diffusion to and degradation in the dendrite (as in *Pde1c*$^{-/-}$ OSNs). Our

modeling suggests the difference between these rates can be several-fold (Fig. 7 and Supplementary note). It is then notable that in *Pde1c*$^{-/-}$ OSNs the termination of EOG responses is even accelerated (Fig. 2). The olfactory transduction system appears to tolerate such a range in the rate of cilial cAMP removal, suggesting that it is not a rate-limiting factor in the termination of OSN responses under normal circumstances, and that other termination mechanisms, namely Ca^{2+}/CaM inhibition of CNG channels18, 23 and Ca^{2+} extrusion24, predominantly determine the kinetics of response termination. Only when cilial cAMP removal is severely hampered, as when the activities of both PDE1C and PDE4A are eliminated, does cAMP removal become rate-limiting.

In wildtype OSNs, the majority of cAMP generated in the cilia, either spontaneously or from odor stimulation, is likely degraded by PDE1C. This scenario is consistent with the fact that *Pde4a*$^{-/-}$ mice display no response deficits. In this case, PDE4A in the dendritic knob functions as a fail-safe for response termination. PDE4A may also prevent odor-evoked cAMP from escaping the dendrite and influencing other cellular processes. That PDE4A may function to spatially restrict cAMP to the cilia is reminiscent of the role of PDE4 enzymes in maintaining cAMP signaling domains in cardiac myocytes (for review, see ref. 15). Techniques to image cAMP in the living cells25 may be useful to further examine cAMP regulation in OSNs.

Although no other PDEs have been reported in canonical OSNs (PDE2 has been found in guanylyl cyclase D-positive neurons in the OE14, 26, 27), OSNs might express other PDE(s) that may account for eventual termination of OSN responses in *Pde1c*$^{-/-}$;*Pde4a*$^{-/-}$ mice. Our cilial PDE activity assays and those of others16 indicate that the activity of unknown PDEs, if any, is unlikely to have a significant effect on olfactory signal transduction.

Pde1c$^{-/-}$ OSNs displayed an unexpected reduction in sensitivity to odor, a paradoxical phenotype for removal of an enzyme that negatively regulates signal transduction. The reduced sensitivity in *Pde1c*$^{-/-}$ OSNs comes, at least in part, from the decrease in the levels of ACIII protein (Fig. 1b), as mice heterozygous for *Adcy3* (coding for ACIII) show reduced EOG amplitudes28. The cause of the decreased ACIII level in *Pde1c*$^{-/-}$ OSNs remains unclear. The reduced sensitivity in *Pde1c*$^{-/-}$ OSNs could also be caused by negative regulation of the activities of signal transduction components. This negative regulation of transduction components is likely to occur even in the absence of odor stimulation. It is well established that the PDE inhibitor IBMX can induce responses in a large portion of OSNs, including 40 – 60% of OSNs in rats and mice7, 29, suggesting that in resting OSNs there is continued production and degradation of cAMP in the cilia, even though they often display low spontaneous electrical activity7, 30, 31. PDE1C, presumably due to its basal catalytic activity, is likely to account for degradation of spontaneously produced cAMP. In *Pde1c*$^{-/-}$ OSNs, the lack of cAMP degradation in cilia would transiently increase cilial cAMP and subsequently cilial Ca^{2+} levels in resting OSNs. Excess Ca^{2+} is expected to negatively regulate the signal transduction pathway20, targeting ACIII19, 32 and the CNG channel23. Regardless of the exact mechanism(s), either reduced ACIII levels, negative feedback on transduction components, or both, the *Pde1c*$^{-/-}$phenotype nevertheless suggests that cilial

PDE activity may indirectly aid in maintaining the signal transduction machinery in a state that is primed for odor response.

It is worth noting that several previously unexplained features of odor responses from IBMX-treated OSNs9 can be interpreted after considering the PDE knockout phenotypes. When bathed in low concentrations of IBMX, OSNs did not show prolonged response termination, but rather showed smaller response amplitudes and slowed onset kinetics9, reminiscent of the *Pde1c*$^{-/-}$ phenotype and highlighting that a basal level of PDE activity may be necessary to maintain OSN sensitivity. When bathed in high concentrations of IBMX, OSNs showed prolonged response termination with reduced response amplitude9, reminiscent of the *Pde1c*$^{-/-}$*;Pde4a*$^{-/-}$ double knockout phenotype.

We also found that PDE1C likely contributes to OSN adaptation to repeated stimulation. Until recently, adaptation to repeated stimulation was attributed mainly to the Ca^{2+}/CaM feedback inhibition on the CNG channel33–36. However, our recent work suggested that Ca^{2+}/CaM-mediated desensitization of the CNG channel has little effect on adaptation to repeated stimulation, but rather contributes to rapid response termination18. An increase in cilial Ca^{2+} as part of the OSN response, in addition to feedback on the CNG channel, likely elevates PDE1C activity through binding with CaM, potentially leading to smaller responses to subsequent stimuli. *Pde1c*$^{-/-}$ OSNs exhibit attenuated adaptation in a paired-pulse stimulation paradigm, consistent with the lack of elevated PDE activity from Ca^{2+}/CaM feedback. It is worth to note that as *Pde1c*$^{-/-}$ OSNs show reduced sensitivity to odors that is reminiscent of already adapted OSNs, the phenotype of attenuated adaptation might also result from a lower ability to further adapt. Interestingly, adaptation to repeated stimulation in *Pde1c*$^{-/-}$*;Pde4a*$^{-/-}$ double knockout mice is not significantly different from the wildtype. This result is consistent with a previous report showing that when the effects of all PDEs were bypassed pharmacologically, OSNs adaptation was not affected21. That eliminating PDE4A masks the adaptation deficit from the loss of PDE1C suggests that the mechanisms by which adaptation is achieved when both PDEs are eliminated (either by genetic or pharmacological means) are substantially different from the wildtype situation, even though the apparent adaptation phenotype is similar. When both PDEs are eliminated, greater recruitment of the remaining adaptation mechanisms, potentially due to additional Ca^{2+} entering the cilia during the prolonged response termination phase, may account for the apparently normal adaptation, whereas in wildtype mice, Ca^{2+}/CaM stimulated PDE1C activity is likely a significant contributor to adaptation.

Response to a sustained stimulation can be viewed as an integration of responses to a series of short stimulations, with the final response determined by a composite of adapted activation and termination mechanisms. *Pde1c*$^{-/-}$ OSNs display a response decline comparable to wildtype OSNs during a sustained stimulation. This result could be superficially understood as the attenuated adaptation to repeated stimulation (i.e. larger subsequent responses) and the faster termination counteracting during sustained stimulation, producing an intermediate response. Therefore, the apparently normal phenotype of adaptation during sustained stimulation in *Pde1c*− /− OSNs is likely determined by a different composition of mechanisms than in wildtype OSNs. It is interesting to compare the phenotype of the *Pde1c*$^{-/-}$ mice to the CNGB1$^{\Delta CaM}$ mice, which carry a mutation that

renders the olfactory CNG channel resistant to Ca^{2+}/CaM-mediated desensitization18. In $CNGB1^{\Delta CaM}$ OSNs, the response decline during sustained stimulation is attenuated, consistent with the reduced ability of these OSNs to terminate the response in combination with the normal adaptation to repeated stimulation. *Pde1c*$^{-/-}$;*Pde4a*$^{-/-}$ OSNs do display a profound deficit in adaptation during sustained stimulation, again consistent with the response being a composite of the phenotypes of prolonged response termination and wildtype-like adaptation to repeated stimulation in these neurons.

METHODS

For all experiments, mice were handled and euthanized with methods approved by the Animal Care and Use Committees of The Johns Hopkins University.

Gene targeting

For *Pde1c*, the targeting vector was designed to delete exons 5–8 (6.7 kilobases genomic DNA on chromosome 6), which encodes the N-terminal portion of the predicted catalytic domain, and to insert a stop codon in the remainder of exon 5 through homologous recombination in embryonic stem cells. For *Pde4a*, the targeting vector was designed to delete exons 9–14 and part of exon 15 (9.9 kilobases genomic DNA on chromosome 9), which encode the entire predicted catalytic domain. Further details of the generation of these knockout mice are provided in Supplementary Figure 1.

Immunohistochemistry

Anesthetized mice were perfused transcardially with 1X PBS followed by 4% (wt/vol) paraformaldehyde. Olfactory tissues were dissected and postfixed for 2 hrs at 4°C followed by cryoprotection in 30% (wt/vol) sucrose overnight at 4°C. Cryosections were cut 14 μm thick and stored at −80°C. Tissue sections were incubated overnight at 4°C with primary antibodies in 1x PBS containing 0.1% (vol/vol) Triton X-100 and 1% (vol/vol) normal donkey serum. After washing, the sections were incubated with secondary antibodies conjugated to either Alexa-488, Alexa-546, or Alexa-647 (Molecular Probes) and imaged by confocal microscopy (LSM 510 Meta, Zeiss) using either a 63x (Fig. 1a) or 100x (Fig. 3a) objective. Images were acquired using the Zeiss LSM software v. 4.2 at 1024 ×1024 pixels resolution, 12 bit-depth, and cropped using Adobe Photoshop. No adjustments to contrast or brightness were made. Primary antibodies were used at the following dilutions: anti-PDE1C213, 14 (kindly provided by Dr. J. Beavo), 1:500; anti-PDE4A13 (kindly provided by Dr. J. Cherry), 1:200; anti-CNGB1b18, 23, 1:200; anti-ACIII (Santa Cruz SC-588), 1:200; anti-OMP (kindly provided by Dr. F. Margolis), 1:1000; anti-Gap43 (Chemicon MAB347), 1:500; anti-acetylated tubulin (Sigma T7451), 1:500.

Western blotting

Olfactory epithelium was dissected and homogenized in 2x Laemmli buffer and stored at −80°C. Tissue homogenates were subjected to SDS-PAGE followed by transfer onto PVDF membrane. Membranes were incubated with blocking buffer (5% (wt/vol) non-fat dry milk in 20 mM Tris, 150 mM NaCl, and 0.1% (vol/vol) Tween-20) for 1 hr at room temperature and then incubated overnight at 4°C with primary antibodies at proper dilutions in blocking

buffer. Membranes were then washed with TBST (20 mM Tris, 150 mM NaCl, and 0.1% Tween-20) followed by incubation with secondary antibodies conjugated to HRP in blocking buffer for 1 hr at room temperature. The blot was visualized with ECL Plus reagent (GE Life Sciences) with detection on a Typhoon 9410 Variable Mode Imager. Primary antibodies were used at the following dilutions: anti-PDE1C, 1:5000; anti-PDE4A, 1:5000; anti-CNGB1b, 1:2000; anti-ACIII, 1:1000; anti-alpha tubulin (Sigma), 1:10,000.

Preparation of OSN cilia and PDE assay

Cilia from OE were isolated by the calcium-shock method37 with slight modifications. Anesthetized mice were perfused transcardially with 1X PBS to minimize blood contamination. The olfactory turbinates were dissected into a buffer containing (in mM) 120 NaCl, 5 KCl, 1.2 $MgCl_2$, 10 HEPES, pH 7.4 and 0.75 mg/ml DTT on ice. $CaCl_2$ stock solution was then added to a final concentration of 10 mM Ca^{2+}. The samples were gently rocked at 4°C for 20 min, followed by centrifugation at 500 rcf for 5 min to pellet de-ciliated epithelia. The supernatant was centrifuged at 18,500 rcf for 20 min to pellet cilia. The cilia pellet was resuspended in BHB buffer (50 mM BES, 0.1 mM EGTA, pH 7.2) plus 0.08 mg/ml DTT and 1x Complete EDTA-free Protease Inhibitor Cocktail (Roche). Protein concentration was determined by the BCA Protein Assay (Pierce).

The PDE activity assay is adapted from Borisy et al., (1992)16. Four μg of OSN cilial protein was incubated with 80,000 cpm ^{3}H-cAMP (GE Life Sciences) for 20 min at 37°C in each of three conditions: 1) in the reaction buffer alone (50 mM BES, 5 mM $MgCl_2$, 0.3 mg/ml BSA, 0.1 mM EGTA, 10 μM unlabelled cAMP); 2) the reaction buffer supplemented with 200 μM Ca^{2+} and 50 nM CaM; and 3) the reaction buffer supplemented with 0.5 mM IBMX (3-isobutyl-1-methylxanthin, ICN Biomedicals). The reaction was stopped by heating to 100°C for 1.5 min and followed by immediate cooling on ice. Subsequently, 1 unit of 5' nucleotidase (Sigma) was added to the reaction (in order to convert the PDE product AMP to adenosine), and the reaction was further incubated at 37°C for 30 min. The reaction was then applied to a 0.5×4 cm column containing 1 ml QAE-Sephadex A25 (Sigma) pre-equilibrated with BHB buffer. The flow-through from two 1.5 ml washes with BHB buffer was collected and mixed with 10 ml of Ultima Gold XR scintillation fluid (Packard Bioscience) followed by assessment of the radioactivity by scintillation counting.

Electroolfactogram

EOG recording was performed essentially as described38. The mouse was sacrificed by CO_2 asphyxiation and decapitated. The head was cut sagittally to expose the medial surface of the olfactory turbinates. The recording electrode, a Ag-AgCl wire in a capillary glass pipette filled with Ringer solution (in mM: 135 NaCl, 5 KCl, 1 $CaCl_2$, 1.5 MgCl, 10 HEPES, pH 7.4) containing 0.5% agarose, was placed on the surface of the OE and connected to a differential amplifier (DP-301, Warner Instruments). EOG signals were recorded from the surface of turbinate IIB and acquired and analyzed with AxoGraph software (Axon Instruments) on a Macintosh computer. The signals were filtered DC-1 kHz and recorded at a sampling rate of 1 kHz. The recorded signals were further low-pass filtered at 25 Hz during analysis. Vapor-phase odorant stimuli were generated by placing 5 ml of odorant solution in a sealed 60 ml glass bottle. This vapor is delivered by a Picospritzer (Parker

Hannifin) as a pulse injected into a continuous stream of humidified air flowing over the tissue sample. All EOG recordings were conducted at room temperature and in mice older than 6 weeks.

For analysis of paired-pulse responses, as the response to the 1st odor pulse has not decayed to baseline at the time the 2nd pulse is given, the recorded 2nd response reflects a sum of the residual 1st response and the "net" response to the 2nd pulse. The net 2nd response peak amplitude was determined by first fitting a trace to the decay phase of the 1st response, and subsequently subtracting the value of this trace at the peak time of the 2nd response from the 2nd pulse peak amplitude18.

Statistical analysis

All statistical significance was determined by unpaired t-test.

Computational Modeling

Computational modeling was performed using the Virtual Cell software from the National Resource for Cell Analysis and Modeling (http://www.vcell.org) (see Supplementary Note online for details).

Supplementary Material

Refer to Web version on PubMed Central for supplementary material.

Acknowledgements

We thank Dr. J. Beavo (Univ. of Washington) for antibody to PDE1C2, Dr. J. Cherry (Boston Univ.) for antibody to PDE4A, and Dr. F. Margolis (Univ. of Maryland) for antibody to OMP. We also thank Drs. L. Brand, R. Cone, S. Hattar, R. Kuruvilla, T. Leinders-Zufall, R. Reed, J. Reisert, and Y. Song for suggestions and comments on experiments and the manuscript, and members of the Hattar-Kuruvilla-Zhao tri-lab of the Department of Biology, Johns Hopkins University for discussion. This work was supported by NIH/NIDCD grant DC009735.

REFERENCES

1. Firestein S, Shepherd GM, Werblin FS. Time course of the membrane current underlying sensory transduction in salamander olfactory receptor neurones. J Physiol. 1990; 430:135–158. [PubMed: 2086763]
2. Lowe G, Gold GH. The spatial distributions of odorant sensitivity and odorantinduced currents in salamander olfactory receptor cells. J Physiol. 1991; 442:147–168. [PubMed: 1798028]
3. Firestein S. How the olfactory system makes sense of scents. Nature. 2001; 413:211–218. [PubMed: 11557990]
4. Ma M. Encoding olfactory signals via multiple chemosensory systems. Crit Rev Biochem Mol Biol. 2007; 42:463–480. [PubMed: 18066954]
5. Kurahashi T, Yau KW. Co-existence of cationic and chloride components in odorant-induced current of vertebrate olfactory receptor cells. Nature. 1993; 363:71–74. [PubMed: 7683113]
6. Kleene SJ. Origin of the chloride current in olfactory transduction. Neuron. 1993; 11:123–132. [PubMed: 8393322]
7. Lowe G, Gold GH. Nonlinear amplification by calcium-dependent chloride channels in olfactory receptor cells. Nature. 1993; 366:283–286. [PubMed: 8232590]
8. Reisert J, Bauer PJ, Yau KW, Frings S. The Ca-activated Cl channel and its control in rat olfactory receptor neurons. J Gen Physiol. 2003; 122:349–363. [PubMed: 12939394]

9. Firestein S, Darrow B, Shepherd GM. Activation of the sensory current in salamander olfactory receptor neurons depends on a G protein-mediated cAMP second messenger system. Neuron. 1991; 6:825–835. [PubMed: 1709025]
10. Boekhoff I, Breer H. Termination of second messenger signaling in olfaction. Proc Natl Acad Sci U S A. 1992; 89:471–474. [PubMed: 1370581]
11. Yan C, et al. Molecular cloning and characterization of a calmodulin-dependent phosphodiesterase enriched in olfactory sensory neurons. Proc Natl Acad Sci U S A. 1995; 92:9677–9681. [PubMed: 7568196]
12. Yan C, Zhao AZ, Bentley JK, Beavo JA. The calmodulin-dependent phosphodiesterase gene PDE1C encodes several functionally different splice variants in a tissue-specific manner. J Biol Chem. 1996; 271:25699–25706. [PubMed: 8810348]
13. Cherry JA, Davis RL. A mouse homolog of dunce, a gene important for learning and memory in Drosophila, is preferentially expressed in olfactory receptor neurons. J Neurobiol. 1995; 28:102–113. [PubMed: 8586960]
14. Juilfs DM, et al. A subset of olfactory neurons that selectively express cGMPstimulated phosphodiesterase (PDE2) and guanylyl cyclase-D define a unique olfactory signal transduction pathway. Proc Natl Acad Sci U S A. 1997; 94:3388–3395. [PubMed: 9096404]
15. Conti M, Beavo J. Biochemistry and physiology of cyclic nucleotide phosphodiesterases: essential components in cyclic nucleotide signaling. Annu Rev Biochem. 2007; 76:481–511. [PubMed: 17376027]
16. Borisy FF, et al. Calcium/calmodulin-activated phosphodiesterase expressed in olfactory receptor neurons. J Neurosci. 1992; 12:915–923. [PubMed: 1312138]
17. Scott JW, Scott-Johnson PE. The electroolfactogram: A review of its history and uses. Microsc Res Tech. 2002; 58:152–160. [PubMed: 12203693]
18. Song Y, et al. Olfactory CNG channel desensitization by Ca2+/CaM via the B1b subunit affects response termination but not sensitivity to recurring stimulation. Neuron. 2008; 58:374–386. [PubMed: 18466748]
19. Leinders-Zufall T, Ma M, Zufall F. Impaired odor adaptation in olfactory receptor neurons after inhibition of Ca2+/calmodulin kinase II. J Neurosci. 1999; 19:RC19. [PubMed: 10407061]
20. Zufall F, Leinders-Zufall T. The cellular and molecular basis of odor adaptation. Chem Senses. 2000; 25:473–481. [PubMed: 10944513]
21. Boccaccio A, Lagostena L, Hagen V, Menini A. Fast adaptation in mouse olfactory sensory neurons does not require the activity of phosphodiesterase. J Gen Physiol. 2006; 128:171–184. [PubMed: 16880265]
22. Chen C, Nakamura T, Koutalos Y. Cyclic AMP diffusion coefficient in frog olfactory cilia. Biophys J. 1999; 76:2861–2867. [PubMed: 10233102]
23. Kaupp UB, Seifert R. Cyclic nucleotide-gated ion channels. Physiol Rev. 2002; 82:769–824. [PubMed: 12087135]
24. Reisert J, Matthews HR. Na+-dependent Ca2+ extrusion governs response recovery in frog olfactory receptor cells. J Gen Physiol. 1998; 112:529–535. [PubMed: 9806962]
25. Willoughby D, Cooper DM. Live-cell imaging of cAMP dynamics. Nat Methods. 2008; 5:29–36. [PubMed: 18165805]
26. Leinders-Zufall T, et al. Contribution of the receptor guanylyl cyclase GC-D to chemosensory function in the olfactory epithelium. Proc Natl Acad Sci U S A. 2007; 104:14507–14512. [PubMed: 17724338]
27. Hu J, et al. Detection of near-atmospheric concentrations of CO2 by an olfactory subsystem in the mouse. Science. 2007; 317:953–957. [PubMed: 17702944]
28. Wong ST, et al. Disruption of the type III adenylyl cyclase gene leads to peripheral and behavioral anosmia in transgenic mice. Neuron. 2000; 27:487–497. [PubMed: 11055432]
29. Ma M, Chen WR, Shepherd GM. Electrophysiological characterization of rat and mouse olfactory receptor neurons from an intact epithelial preparation. J Neurosci Methods. 1999; 92:31–40. [PubMed: 10595701]
30. Kurahashi T. Activation by odorants of cation-selective conductance in the olfactory receptor cell isolated from the newt. J Physiol. 1989; 419:177–192. [PubMed: 2621628]

31. Firestein S, Werblin F. Odor-induced membrane currents in vertebrate-olfactory receptor neurons. Science. 1989; 244:79–82. [PubMed: 2704991]
32. Wei J, et al. Phosphorylation and inhibition of olfactory adenylyl cyclase by CaM kinase II in Neurons: a mechanism for attenuation of olfactory signals. Neuron. 1998; 21:495–504. [PubMed: 9768837]
33. Chen TY, Yau KW. Direct modulation by Ca(2+)-calmodulin of cyclic nucleotideactivated channel of rat olfactory receptor neurons. Nature. 1994; 368:545–548. [PubMed: 7511217]
34. Kurahashi T, Menini A. Mechanism of odorant adaptation in the olfactory receptor cell. Nature. 1997; 385:725–729. [PubMed: 9034189]
35. Bradley J, Reuter D, Frings S. Facilitation of calmodulin-mediated odor adaptation by cAMP-gated channel subunits. Science. 2001; 294:2176–2178. [PubMed: 11739960]
36. Munger SD, et al. Central role of the CNGA4 channel subunit in Ca2+-calmodulindependent odor adaptation. Science. 2001; 294:2172–2175. [PubMed: 11739959]
37. Anholt RR, Aebi U, Snyder SH. A partially purified preparation of isolated chemosensory cilia from the olfactory epithelium of the bullfrog, Rana catesbeiana. J Neurosci. 1986; 6:1962–1969. [PubMed: 3525776]
38. Zhao H, et al. Functional expression of a mammalian odorant receptor. Science. 1998; 279:237–242. [PubMed: 9422698]

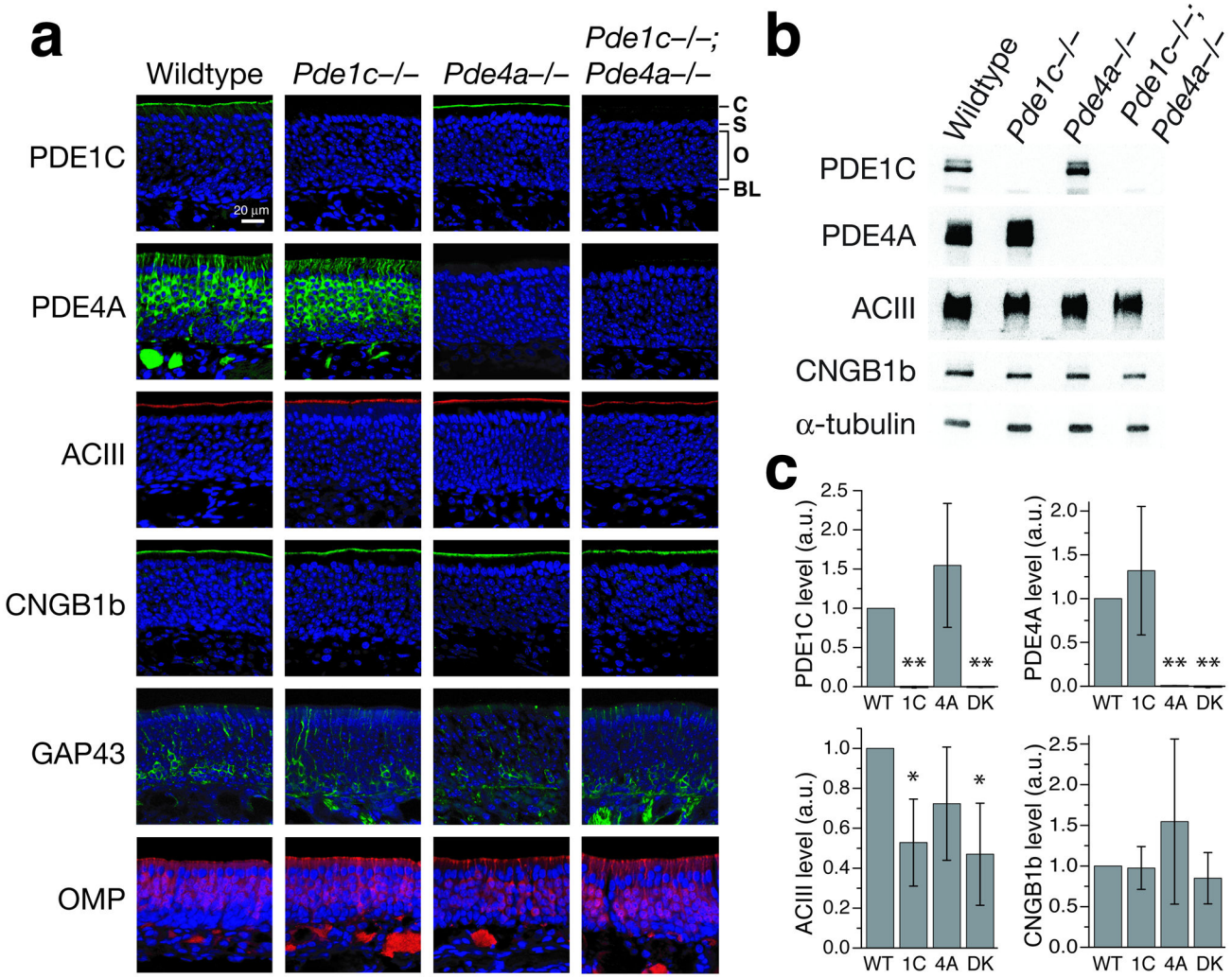

Figure 1. Molecular characterization of *Pde1c*$^{-/-}$, *Pde4a*$^{-/-}$, and *Pde1c*$^{-/-}$;*Pde4a*$^{-/-}$ mice

(a) Immunostaining on sections of olfactory epithelium. Sections were counterstained with DAPI (blue) to label cell nuclei. C, cilial layer; S, supporting cell layer; O, olfactory sensory neuron layer; BL, basal lamina. Scale bar: 20 μm. (b and c) Western blot analysis of total OE proteins. (b) Example Western blots for PDE1C, PDE4A, ACIII, and CNGB1b on total OE proteins from all four genotypes. α-tubulin is used as a loading control. (c) Quantification of Western blotting. Values are normalized to α-tubulin staining and shown relative to wildtype in arbitrary units (a.u.). PDE1C is detected at similar levels in wildtype and *Pde4a*$^{-/-}$ mice (1.55 ± 0.79), but is undetectable in *Pde1c*$^{-/-}$ and *Pde1c*$^{-/-}$;*Pde4a*$^{-/-}$ mice. PDE4A is detected at similar levels in wildtype and *Pde1c*$^{-/-}$ mice (1.32 ± 0.73), but is undetectable in *Pde4a*$^{-/-}$ and *Pde1c*$^{-/-}$;*Pde4a*$^{-/-}$ mice. ACIII levels are significantly reduced in *Pde1c*$^{-/-}$ (0.52 ± 0.22) and *Pde1c*$^{-/-}$;*Pde4a*$^{-/-}$ mice (0.47 ± 0.26), but not in *Pde4a*$^{-/-}$ mice (0.72 ± 0.28). CNGB1b levels are similar in all genotypes (*Pde1c*$^{-/-}$, 0.97 ± 0.26; *Pde4a*$^{-/-}$, 1.55 ± 1; *Pde1c*$^{-/-}$;*Pde4a*$^{-/-}$, 0.85 ± 0.31). Data are the average of 3 independent sets of mice, each set consisting of a mouse of each genotype. Error bars are 95% confidence intervals (CI). Statistical significance was determined by one-sample t-test.

* $P < 0.05$, ** $P < 0.01$. WT, wildtype; 1C, *Pde1c−/*; 4A, *Pde4a*$^{-/-}$; DK, *Pde1c*$^{-/-}$*;Pde4a*$^{-/-}$.

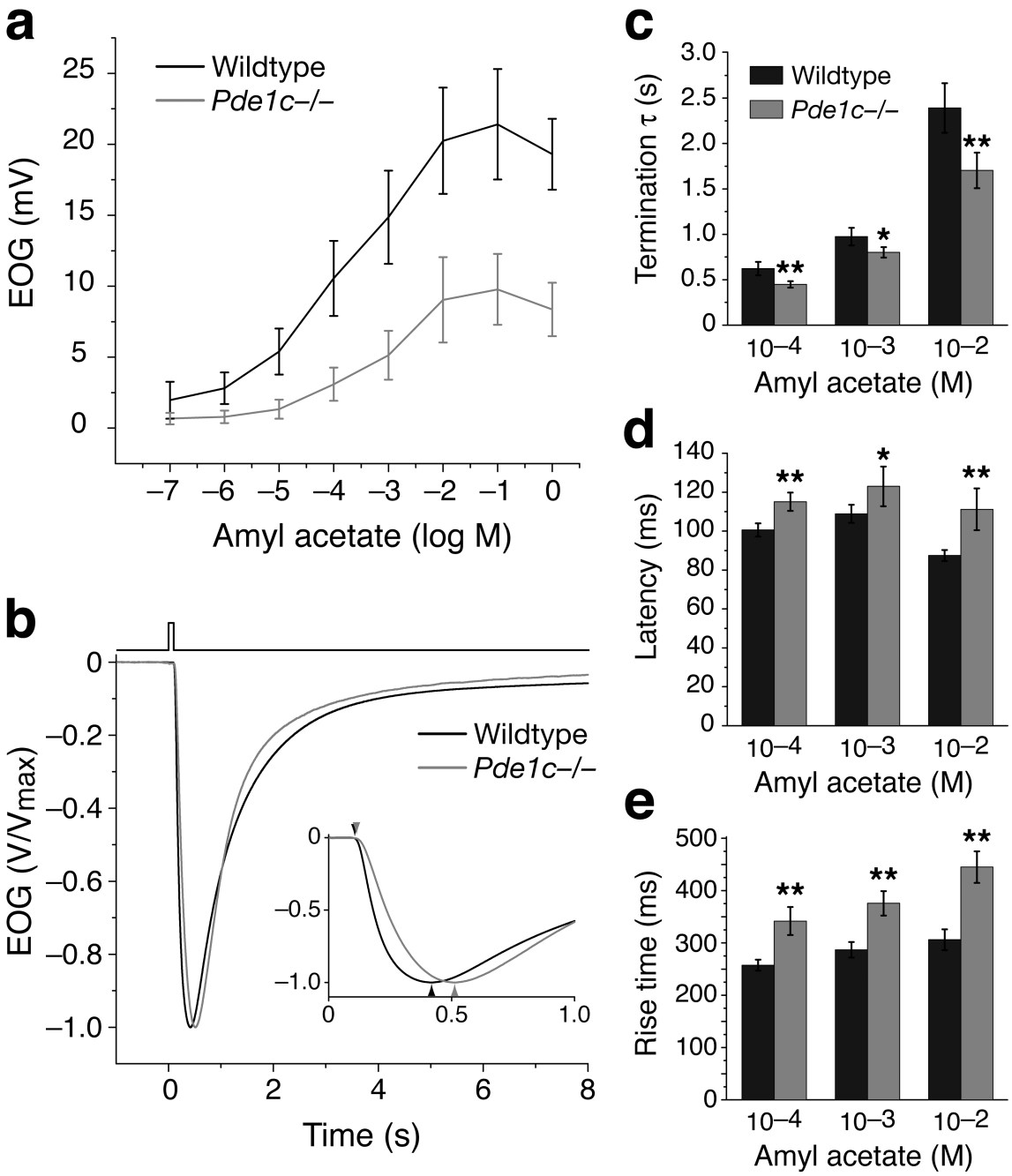

Figure 2. *Pde1c*$^{-/-}$ OSNs display reduced EOG amplitude, faster response termination, and slower onset kinetics

(a) Dose-response relations of EOG responses to amyl acetate from wildtype (n = 7) and *Pde1c*$^{-/-}$ (5) mice. Amyl acetate was delivered as 100 ms pulses. Concentrations on the X-axis are those of the liquid solution. Data points are linked with straight lines; error bars are SD. (b) EOG responses to a single 100 ms pulse of 10^{-3} M amyl acetate. Responses are normalized and averaged for comparison of response kinetics (Wildtype, n = 15; *Pde1c*$^{-/-}$, 10). Inset shows the traces plotted on an expanded time axis. (c) Termination time constants (τ), determined by a single exponential fit to the decay phase of the EOG signal. For 10^{-4}

M, 10^{-3} M, and 10^{-2} M, $P = 9.7x10^{-4}$, 0.011, and 8.4×10^{-4}; wildtype, $n = 20$; *Pde1c*$^{-/-}$, $n = 14$. (d) Response latencies, defined as the time between the initiation of odor pulse and the start of the response (1% of peak amplitude). For 10^{-4} M, 10^{-3} M, and 10^{-2} M, $P = 4.5\times10^{-5}$, 0.011, and 5.1×10^{-5}; wildtype, $n = 15$; *Pde1c*$^{-/-}$, $n = 10$. (e) Response rise times, defined as the time from the start of the response to the peak. For 10^{-4} M, 10^{-3} M, and 10^{-2} M, $P = 1.1\times10^{-6}$, 9.0×10^{-7}, 5.8×10^{-8}; wildtype, $n = 15$; *Pde1c*$^{-/-}$, $n = 10$. In (c–e), error bars are 95% CI. *P* values are from unpaired t-tests. *, $P < 0.05$; **, $P < 0.01$.

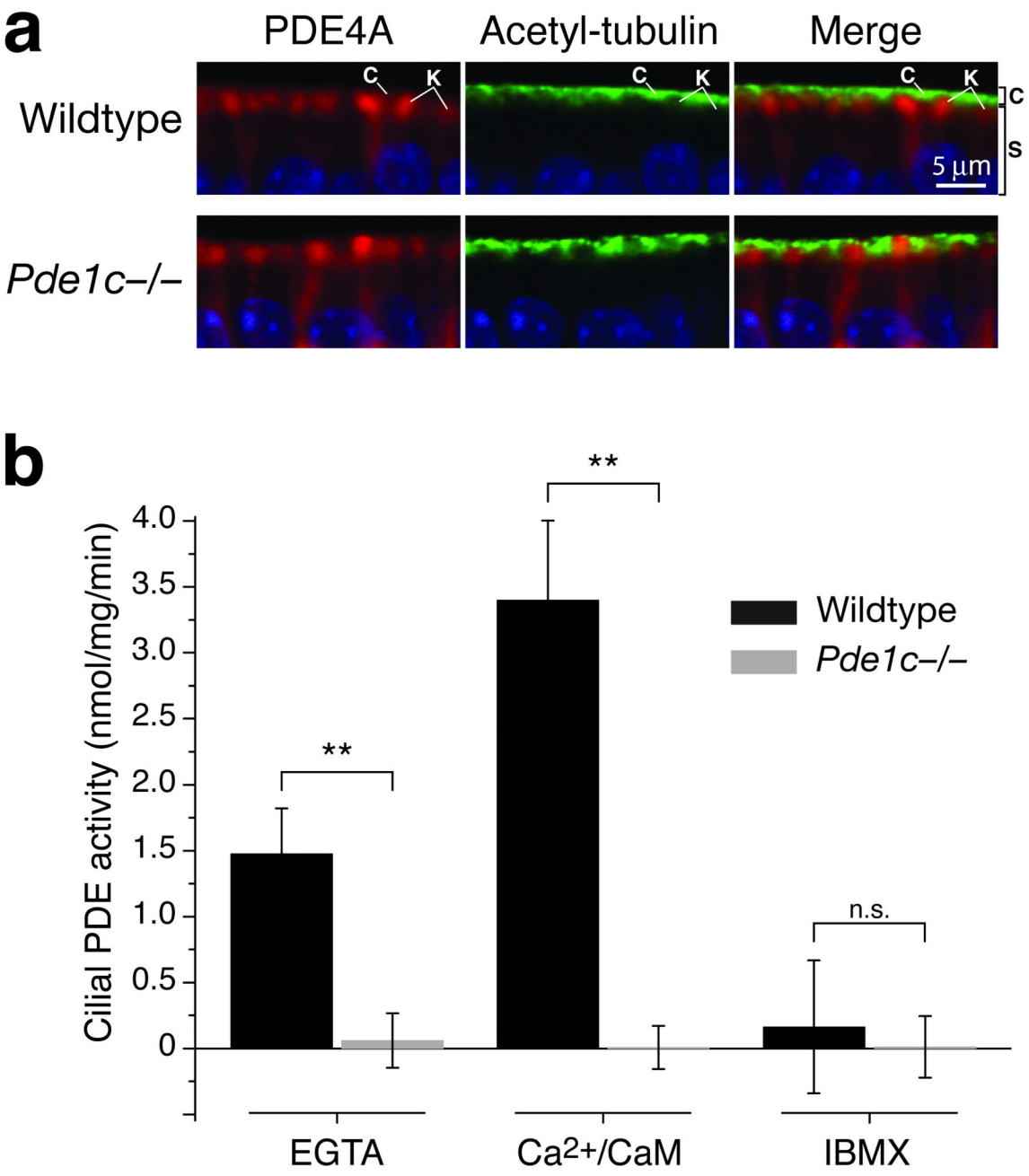

Figure 3. Knockout of PDE1C eliminates all PDE activity from OSN cilia

(a) Co-immunostaining for PDE4A (red) and the cilia marker acetylated tubulin (green) on sections of OE from wildtype and *Pde1c*$^{-/-}$ mice. Shown are apical portions of the OE under high magnification. In both wildtype and *Pde1c*$^{-/-}$ mice, immunoreactivity for PDE4A and acetylated tubulin appears in distinct spatial domains. C, cilial layer; K, dendritic knobs; S, supporting cell layer. Sections are counterstained with DAPI. Scale bar: 5 µm. (b) PDE catalytic activity assay in cilia preparations from wildtype and *Pde1c*$^{-/-}$ mice. PDE activity in wildtype cilia was increased by addition of Ca^{2+}/CaM and inhibited

by addition of IBMX. Activity from *Pde1c*$^{-/-}$ cilia under all conditions was virtually undetectable, similar to wildtype cilia treated with IBMX. Error bars are 95% CI. Data for each genotype are the average of 5 independent preparations (mice). Each preparation was assayed in duplicate.

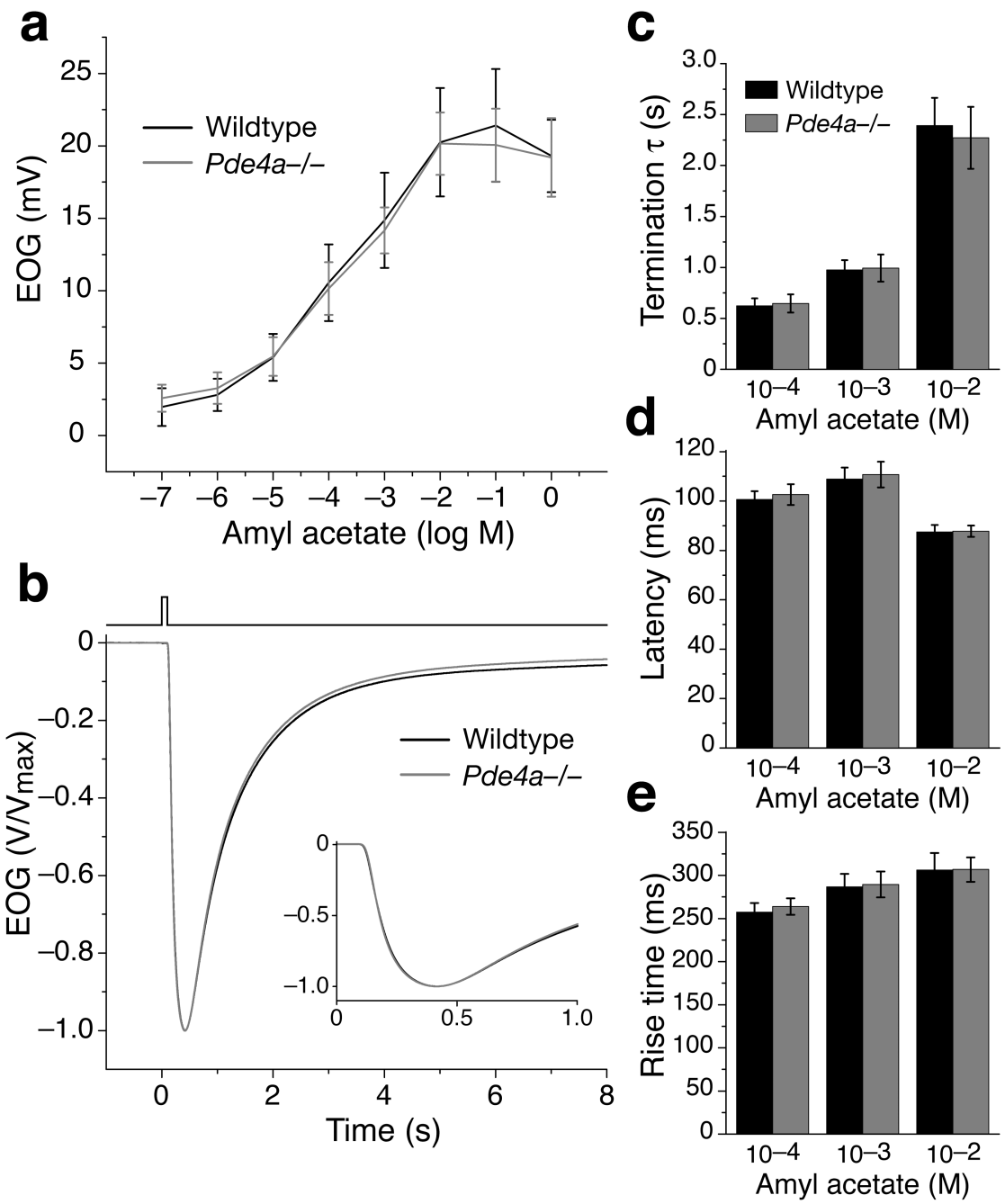

Figure 4. *Pde4a*$^{-/-}$ OSNs display no aberrant EOG response properties

Data for wildtype mice is re-plotted from Figure 2 for reference. (a) Dose-response relationship of EOG responses to amyl acetate from *Pde4a*$^{-/-}$ mice (n = 5). Error bars are SD. (b) Normalized and averaged EOG responses from *Pde4a*$^{-/-}$ mice (n = 14) to a single 100 ms pulse of 10^{-3} M amyl acetate. Inset shows the traces plotted on an expanded time axis. (c) Termination τ for responses to three amyl acetate concentrations. For 10^{-4} M, P = 0.70; 10^{-3} M, P = 0.82; 10^{-2} M, P = 0.57. (d) Response latencies. For 10^{-4} M, P = 0.47; 10^{-3} M, P = 0.61; 10^{-2} M, P = 0.87. (e) Response rise times. For 10^{-4} M, P = 0.39; 10^{-3} M,

$P = 0.81$; 10^{-2} M, $P = 0.97$. In (c–e), error bars are 95% CI. All P values are from unpaired t-tests, $n = 14$ for *Pde4a*$^{-/-}$. No significant differences ($P < 0.05$) are found in any parameters.

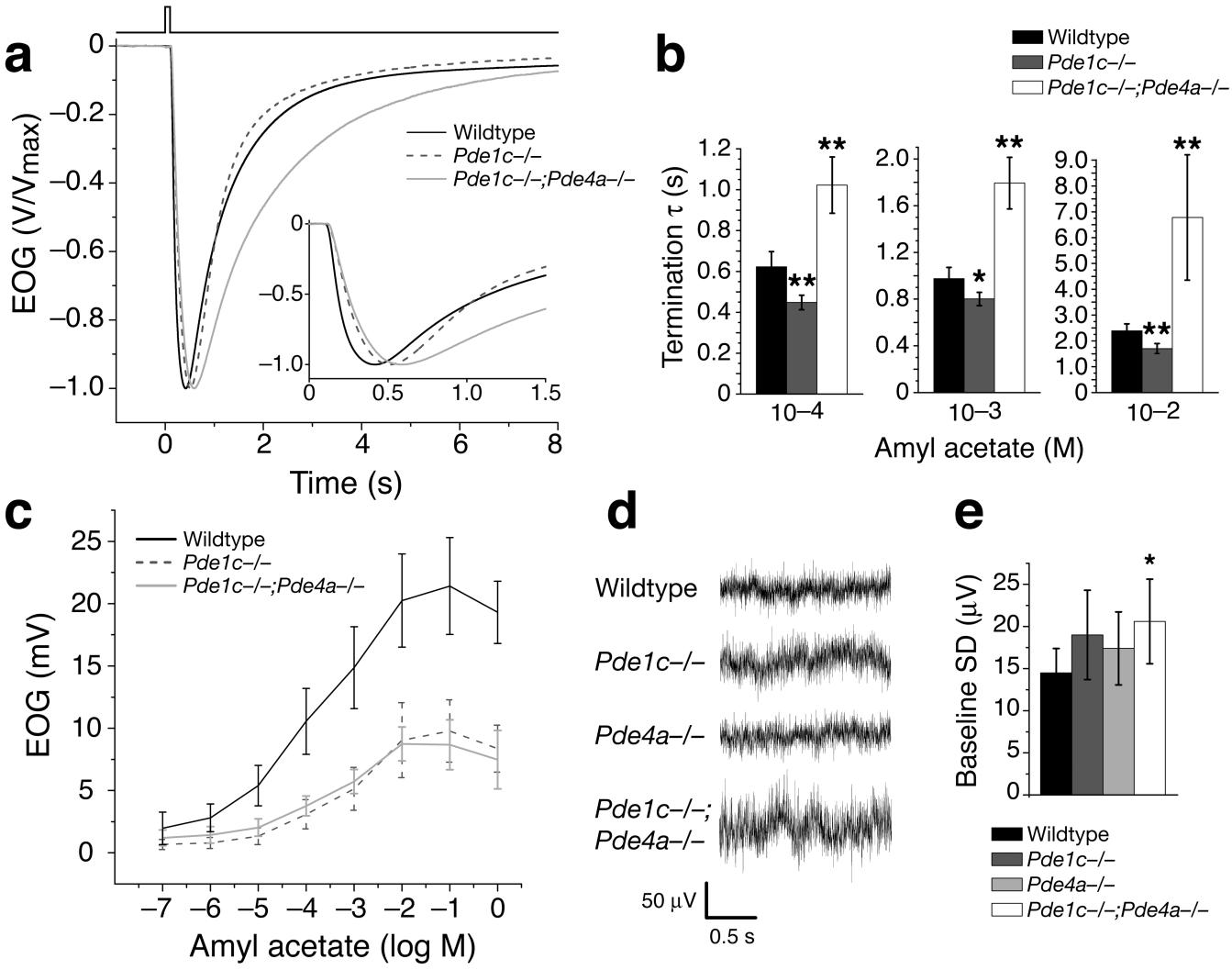

Figure 5. *Pde1c*$^{-/-}$;*Pde4a*$^{-/-}$ double knockout mice display prolonged response termination and increased baseline noise

Data for wildtype and *Pde1c*$^{-/-}$ mice are re-plotted from Figure 2 for reference. (a) Normalized and averaged EOG responses from *Pde1c*$^{-/-}$;*Pde4a*$^{-/-}$ (n = 17) mice to a single 100 ms pulse of 10^{-3} M amyl acetate. Inset shows the traces plotted on an expanded time axis. (b) Termination τ for responses to three amyl acetate concentrations. Responses from *Pde1c*$^{-/-}$;*Pde4a*$^{-/-}$ mice have significantly longer termination τ compared to wildtype. Error bars are 95% CI. For 10^{-4} M, $P = 8.3\times10^{-6}$; 10^{-3} M, $P = 3.5\times10^{-8}$; 10^{-2} M, $P = 5.2\times10^{-4}$; all unpaired t-tests with the wildtype, n = 17 for *Pde1c*$^{-/-}$;*Pde4a*$^{-/-}$. (c) Dose-response relationship for amyl acetate from *Pde1c*$^{-/-}$;*Pde4a*$^{-/-}$ mice (n = 8). Error bars are SD. (d) Representative baseline traces (filtered DC - 1 kHz) from each genotype. (e) Baseline noise is quantified as the standard deviation in the voltage from 2 s of recording (sampling rate 2 kHz) without stimulation. *Pde1c*$^{-/-}$;*Pde4a*$^{-/-}$ mice display significantly increased baseline noise compared to wildtypes. Error bars are 95% CI. Compared with wildtype: *Pde1c*$^{-/-}$, P = 0.144; *Pde4a*$^{-/-}$, P = 0.278; *Pde1c*$^{-/-}$;*Pde4a*$^{-/-}$, P = 0.048; all

unpaired t-tests, $n = 12$ for wildtype, $n = 10$ for *Pde1c*$^{-/-}$, $n = 7$ for *Pde4a*$^{-/-}$, $n = 11$ for *Pde1c*$^{-/-}$;*Pde4a*$^{-/-}$. * indicates $P < 0.05$, ** indicates $P < 0.01$.

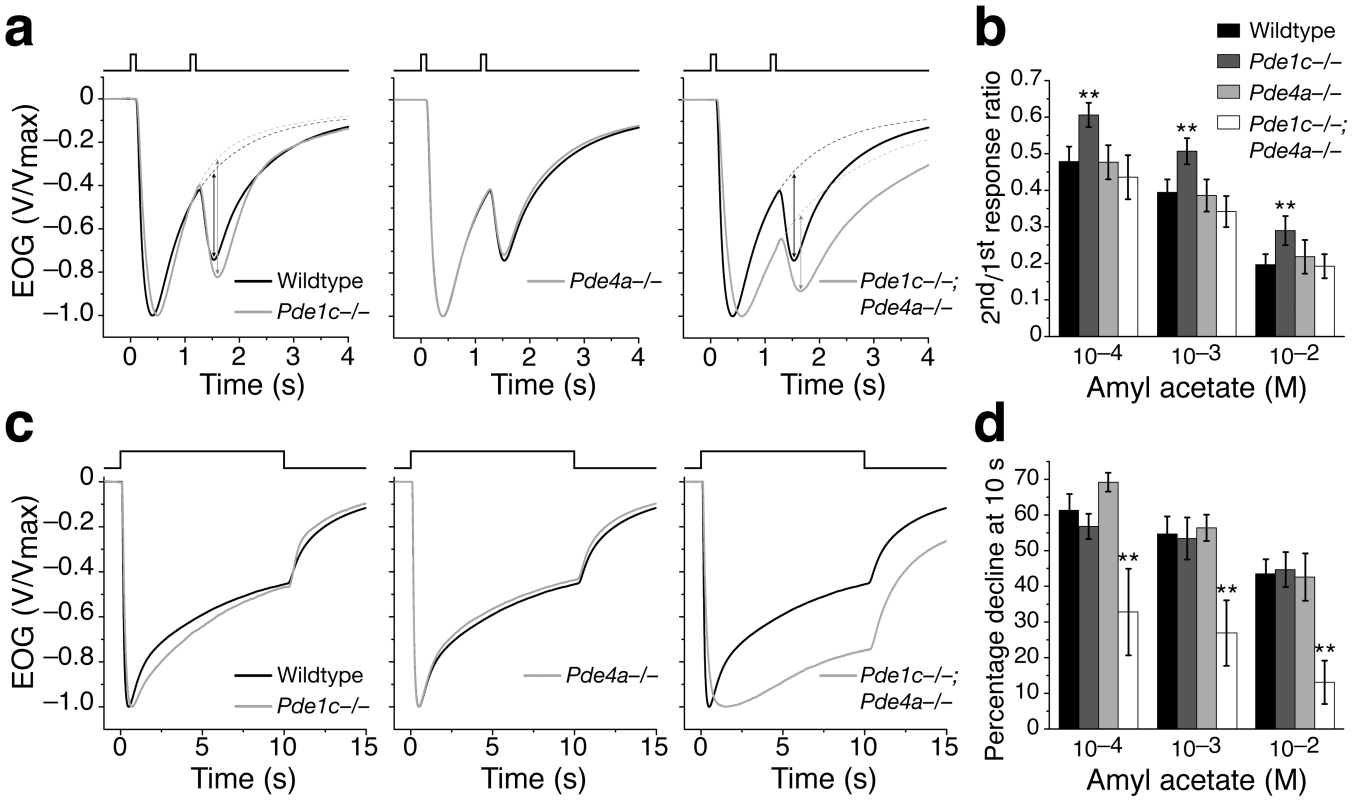

Figure 6. OSN adaptation is differently affected in *Pde1c*$^{-/-}$ and *Pde1c*$^{-/-}$;*Pde4a*$^{-/-}$ mice

(a) Normalized and averaged EOG responses from wildtype (n = 13), *Pde1c*$^{-/-}$ (9), *Pde4a*$^{-/-}$ (8), and *Pde1c*$^{-/-}$;*Pde4a*$^{-/-}$ (8) mice to two 100 ms pulses of 10^{-3} M amyl acetate separated by a 1 s interval. The contribution of the residual 1st response was removed from the recorded 2nd response to obtain the net 2nd response peak amplitude (see Methods), as indicated by the arrows on the *Pde1c*$^{-/-}$ and *Pde1c*$^{-/-}$;*Pde4a*$^{-/-}$ traces. (b) Ratio of 2nd net peak amplitude to the 1st peak amplitude. For *Pde1c*$^{-/-}$ compared to wildtype, P = 2.6×10^{-4}, 3.9×10^{-4}, and 0.0011 for 10^{-4}, 10^{-3}, and 10^{-2} M respectively. For *Pde4a*$^{-/-}$ compared to wildtype, P = 0.95, 0.77, and 0.42. For *Pde1c*$^{-/-}$;*Pde4a*$^{-/-}$ compared to wildtype, P = 0.23, 0.071, and 0.85. (c) Normalized and averaged EOG responses to a 10 s pulse of 10^{-3} M amyl acetate from wildtype (n = 15), *Pde1c*$^{-/-}$ (10), *Pde4a*$^{-/-}$ (6), and Pde1c$^{-/-}$;Pde4a$^{-/-}$ (9) mice. (d) Response decline during stimulation, quantified by the percent reduction in the peak amplitude at the 10 s time point. For *Pde1c*$^{-/-}$ compared to wildtype, P = 0.18, 0.74, and 0.73 for 10^{-4}, 10^{-3}, and 10^{-2} M respectively. For *Pde4a*$^{-/-}$ compared to wildtype, P = 0.056, 0.67, and 0.80. For *Pde1c*$^{-/-}$;*Pde4a*$^{-/-}$ compared to wildtype, $P = 4.5\times10^{-5}$, 8.3×10^{-6}, and 1.7×10^{-8}. In (b) and (d), error bars are 95% CI and P values are from unpaired t-tests. * indicates $P < 0.05$, ** indicates $P < 0.01$.

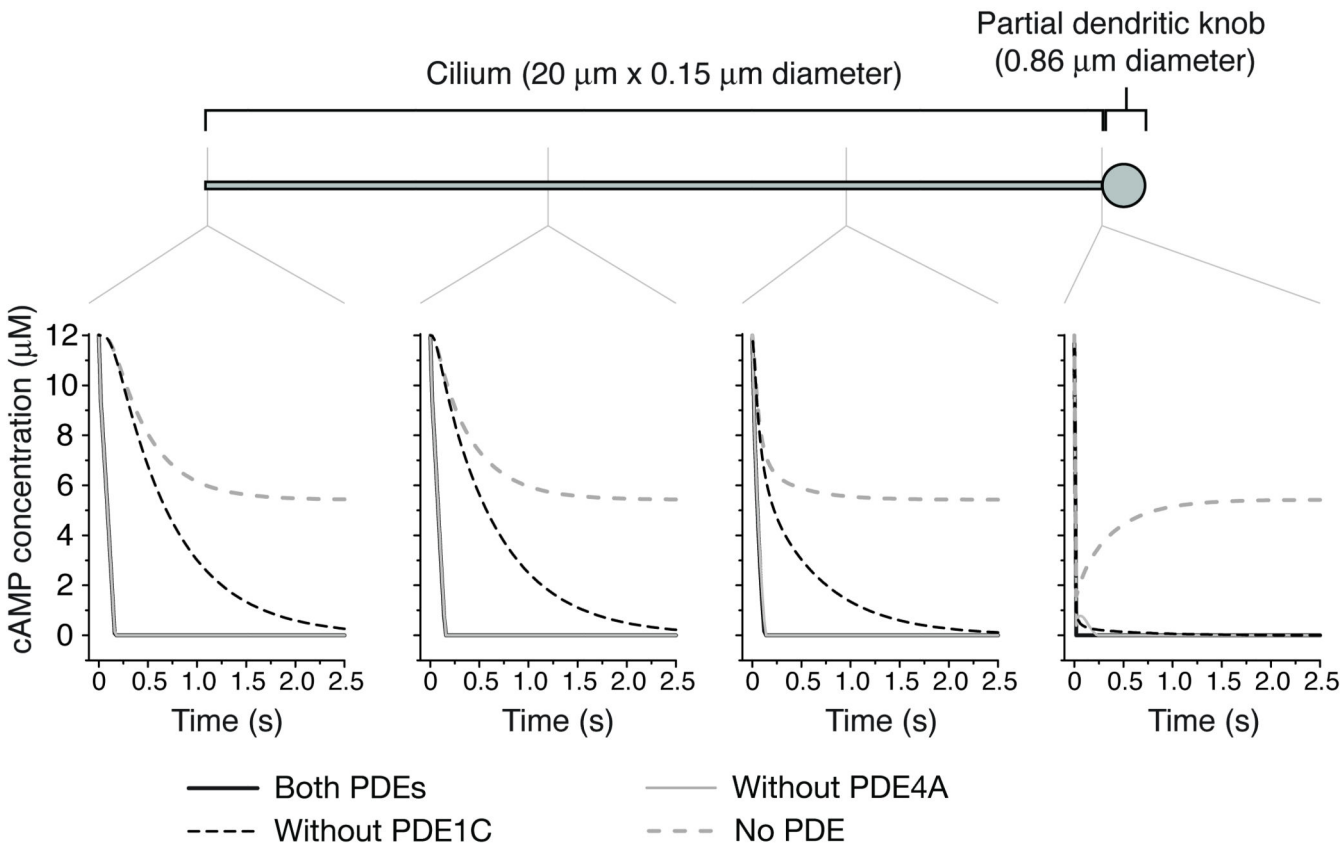

Figure 7. Computer modeling of degradation and diffusion of cilial cAMP

A cilium is attached to a "mini-knob", which has approximately 1/12 of the volume of a 2 μm diameter dendritic knob (an estimation of the volume of the knob that would be available to a single cilium). The cilium is initially filled with 12 μM cAMP, a concentration that saturates the olfactory CNG channels. Four scenarios were modeled: with activities of both PDEs (modeling wildtype); without PDE4A activity; without PDE1C activity; and without any PDE activity (modeling *Pde1c*$^{-/-}$;*Pde4a*$^{-/-}$ OSNs). Diffusion of cAMP is included in all scenarios. The change in cAMP concentrations is shown at four points along the model cilium for each scenario. Note that the black lines (wildtype modeling) are obscured by the light gray lines (modeling without PDE4A). For further details see the Supplementary note online.

Nat Neurosci. Author manuscript; available in PMC 2009 October 01.

Table 1

Analysis of EOG responses (Amyl Acetate stimulation)

			Wildtype	*Pde1c−/−*	*Pde4a−/−*	*Pde1c−/−:Pde4a−/−*
Response to Single Pulse	Maximum amplitude (mV)		21.4 ± 3.9 (7)	9.8 ± 2.5 (5) **	20.2 ± 2.1 (5)	8.7 ± 1.4 (8) **
	Latency (ms)	10^{-4} M	100.6 ± 3.4 (15)	115.1 ± 4.7 (10) **	102.6 ± 4.2 (14)	116.4 ± 3.9 (17) **
		10^{-3} M	108.8 ± 4.7 (15)	123.0 ± 10 (10) *	110.7 ± 5.2 (14)	125.0 ± 4.5 (17) **
		10^{-2} M	87.5 ± 2.8 (15)	111.2 ± 11 (10) **	87.8 ± 2.3 (14)	118.9 ± 8.7 (17) **
	Rise time (ms)	10^{-4} M	257 ± 11 (15)	341 ± 27 (10) **	264 ± 10 (14)	405 ± 13 (17) **
		10^{-3} M	287 ± 15 (15)	376 ± 23 (10) **	289 ± 15 (14)	441 ± 19 (17) **
		10^{-2} M	306 ± 20 (15)	445 ± 30 (10) **	307 ± 14 (14)	562 ± 25 (17) **
	Termination τ(s)	10^{-4} M	0.62 ± 0.07 (20)	0.45 ± 0.04 (14) **	0.65 ± 0.09 (14)	1.02 ± 0.14 (17) **
		10^{-3} M	0.97 ± 0.10 (20)	0.80 ± 0.06 (14) *	0.99 ± 0.13 (14)	1.79 ± 0.22 (17) **
		10^{-2} M	2.39 ± 0.27 (20)	1.70 ± 0.20 (14) **	2.27 ± 0.30 (14)	6.78 ± 2.43 (17) **
Adaptation	Paired–pulse: ratio of 2nd pulse to 1st pulse	10^{-4} M	0.48 ± 0.04 (13)	0.61 ± 0.03 (9) **	0.48 ± 0.05 (8)	0.44 ± 0.06 (8)
		10^{-3} M	0.39 ± 0.04 (13)	0.51 ± 0.04 (9) **	0.39 ± 0.04 (8)	0.34 ± 0.04 (8)
		10^{-2} M	0.20 ± 0.03 (13)	0.29 ± 0.04 (9) **	0.22 ± 0.05 (8)	0.19 ± 0.03 (8)
	Sustained pulse: % decline at 10 s	10^{-4} M	61.3 ± 4.6 (15)	56.8 ± 3.5 (10)	69.2 ± 2.6 (6)	32.8 ± 12.2 (9) **
		10^{-3} M	54.7 ± 4.9 (15)	53.4 ± 5.9 (10)	56.4 ± 3.7 (6)	26.9 ± 9.2 (9) **
		10^{-2} M	43.5 ± 4.1 (15)	44.7 ± 4.9 (10)	42.6 ± 6.7 (6)	13.1 ± 6.1 (9) **

Odorant concentrations are for amyl acetate. For maximum amplitude, values are ± SD; for all others, values are ± 95% CI. The number of mice *(n)* is indicated in parentheses.

* indicates $P < 0.05$ in an unpaired t–test compared to wildtype,

** indicates $P < 0.01$.